Nuclear Instruments and Methods in Physics Research A 673 (2012) 16–21

Contents lists available at SciVerse ScienceDirect

Nuclear Instruments and Methods in Physics Research A

journal homepage: www.elsevier.com/locate/nima

Measurement of (n,α) reactions on ^{147}Sm and ^{149}Sm using a lead slowing-down spectrometer

J.T. Thompson [a,*], T. Kelley [b], E. Blain [a], R.C. Haight [c], J.M. O'Donnell [c], Y. Danon [a]

[a] Department of Mechanical, Aerospace and Nuclear Engineering, Rensselaer Polytechnic Institute, Troy, New York 12180, USA
[b] Department of Physics, Applied Physics and Astrophysics Rensselaer Polytechnic Institute, Troy, New York 12180, USA
[c] Los Alamos Neutron Science Center Los Alamos National Laboratory, Los Alamos, New Mexico 87545, USA

ARTICLE INFO

Article history:
Received 7 October 2011
Received in revised form
28 December 2011
Accepted 4 January 2012
Available online 12 January 2012

Keywords:
(n,α)
Lead slowing-down spectrometer
Digitizer
Compensated detectors
Samarium
Sm-147
Sm-149

ABSTRACT

The lead slowing-down spectrometer (LSDS) at Rensselaer Polytechnic Institute (RPI) was used to extend previous measurements of the (n,α) cross section on ^{147}Sm and perform measurements on ^{149}Sm over the energy range 0.1 eV–10 keV. A compensated detector based on passivated implanted planar silicon (PIPS) detectors was constructed. Signals from two detectors were combined in opposite polarity and digitized providing a single detector capable of discriminating against capture γ's and "γ-flash" while preserving the discrete signals produced by α events and providing a simultaneous background measurement. Extrapolating the results predicts a 0.3 ± 0.3 mbarn and 11.5 ± 1.1 mbarn thermal neutron (n,α) cross section for ^{147}Sm and ^{149}Sm, respectively. This measurement provides new information on (n,α) reaction cross sections. The method of measuring neutron induced charged particle emission cross sections presented here can be expanded to more isotopes of interest to reactor engineers or astrophysicists, as well as to (n,p) reactions.

1. Introduction

To understand stellar processes and isotopic abundances accurate knowledge of nuclear reaction rates is needed [1,2]. Although models exist to predict these cross sections [3–6] they need the constraints of experimental data [7]. The success of applying results from α scattering experiments have been limited because coulomb interaction prevents direct measurement at incident energies relevant to astrophysics [7]. Stellar chemical evolution models and predictions of nucleosynthesis rates of the proton rich p-process isotopes are very sensitive to α+nucleus potentials. These potentials are energy and target sensitive and as a result predictions suffer greatly from a lack of experimental data to test against [8].

To perform measurements of low cross section reactions, large sample masses are often employed. Because of their short range, direct measurement of α particles emitted by the sample requires the samples to be thin, typically having a maximum thickness of a few mg/cm^2. These contradictory requirements are normally met using very large area samples [7,9]. Even with large sample areas, measurement times can remain long due to low fluxes typically employed in time of flight (ToF) methods. Even with the possibility of large samples, some isotopes are not easily available in the large quantities needed due to very low natural abundances of stable isotopes or activity for radioisotopes.

The lead slowing-down spectrometer (LSDS) is a unique tool in that the flux from a pulsed neutron source is amplified by $\sim 10^4$ over the more conventional ToF methods [10] allowing for smaller samples and shorter measurement times. The average neutron energy, $\overline{E}$, follows the time dependent equation

$$\overline{E} = \frac{k}{(t+t_0)^2}, \tag{1}$$

where t is the neutron slowing-down time and the two constants vary slightly between spectrometers but for the LSDS installed at Rensselaer Polytechnic Institute (RPI), also known as the Rensselaer Intense Neutron Source (RINS), $t_0 = 0.3$ μs and $k = 165$ keV μs^2 [13]. The flux profile used here is given by Fisher [14] as

$$\phi = \overline{E}^{-a} e^{-\sqrt{b/\overline{E}}}, \tag{2}$$

where $a = 0.776$, $b = 0.214$. $\overline{E}$ and ϕ are in units of eV and cm^{-2} eV^{-1}, respectively.

The LSDS produces a large neutron flux with a broad energy resolution. The neutron population starts in an evaporation energy spectrum but immediately begins to focus on the function given by Eq. (1) because the faster neutrons will on average scatter sooner and lose more energy per collision than the slower neutrons. This focusing effect is not perfect and reaches a

* Corresponding author. Tel.: +1 518 276 4115, fax: +1 518 276 4832.
E-mail address: thompj@rpi.edu (J.T. Thompson).

0168-9002/$ - see front matter © 2012 Elsevier B.V. All rights reserved.
doi:10.1016/j.nima.2012.01.005

minimum full width at half max (FWHM) of ~30% when the average neutron energy is ~1 keV. Below a few eV's, the thermal motion of the lead nuclei begin to degrade the resolution [10]. The resolution of the RPI LSDS has been found to be [13]

$$\left(\frac{\Delta E}{\overline{E}}\right)_{FWHM} = \sqrt{\frac{0.128}{\overline{E}} + 0.0835 + 3.05 \times 10^{-5}\overline{E}}. \quad (3)$$

In this report, results from the first use of the LSDS at RPI for (n,α) cross section measurements will be shown. We have chosen to study (n,α) reactions on ^{147}Sm and ^{149}Sm. These reactions have been identified [11,12] as important in astrophysics in the keV energy range. Furthermore, these isotopes are fission products and so these reactions could be important both for thermal and fast reactors. LSDS experiments can cover the range from below 1 eV to 10's of keV and therefore provide data for these applications.

2. Experimental set-up

2.1. LSDS

The LSDS at RPI consists of 72 *t* (a 1.8 m cube) of 99.99% [15] pure lead. At its center are several air cooled tantalum plates making up the neutron producing target. The LSDS is attached to the end of the Gaerttner Electron Linear Accelerator Facility (LINAC). The target is bombarded with electrons with energy up to ~60 MeV which produced Bremsstrahlung radiation that then undergoes (γ,n) reactions producing neutrons with an evaporation spectrum [15]. Neutrons scatter through the lead losing energy through inelastic collisions until dropping below the inelastic threshold of lead, at which point they continue to lose energy through elastic collisions.

During this work, the LINAC was operated at an average beam current of 13 μA and at 55 MeV. The detector was placed in a channel in the lead, ~20 cm below the target and ~40 cm deep. The channel was back filled with 10 cm of lead and covered with a sheet of cadmium. Data were collected from ^{147}Sm and ^{149}Sm for 4.77 h and 12.74 h, respectively.

2.2. Samples

Two samples were prepared from isotopically enriched samarium oxide (Sm_2O_3), see Table 1 for isotopic composition. Sm_2O_3 was reacted with concentrated nitric acid forming $Sm(NO_3)_3$. The heat released during this reaction was enough to boil away most of the water so the remaining material was dissolved in deionized water until no sediment remained after sitting overnight. The solution was stippled to 99.9% aluminum disks forming ~1 cm diameter circles. To ensure that all of the samarium nitrate was deposited the container was rinsed with deionized water which was also stippled to the sample. These samples were left on a hot plate turned to high for a day to reduce the water mass in the sample. The samarium nitrate partially decomposed back to samarium oxide prior to the experiment. Sample thickness is a combination of samarium oxide, samarium nitrate, un-reacted nitrate and water left in the crystal structure so the mass of the sample was measured again to determine the sample thickness. Mass of the samarium in the sample was derived from the mass of the oxide initially used. Table 2 contains all of the sample parameters.

2.3. Detector and electronics

The two PIPS detectors (Canberra model PD-150-30-40EPI-40) were arranged in a light tight aluminum shell facing each other. The sample was placed between the two detectors with a 2 mm air gap between the sample and the active surface of the detector. Fig. 1 is a photograph of the detector chamber. The PIPS detectors have an active surface area of 150 mm^2 and a depletion depth of 40 μm with the applied +20 V bias.

The neutron pulse was preceded by a very strong burst of γ-rays or "γ-flash." In order to minimize the effect of the "γ-flash" a compensating circuit was placed before the preamp, shown in Fig. 2. Signals were extracted through a 4.7 nF capacitor and sent though a Phillips Scientific 460 inverting transformer, one of these transformers was modified so that it was non-inverting. Signals were then combined and coupled to the input of a Cremat CR-110 preamplifier modified to have a 45 ns decay time though another 4.7 nF capacitor. The output of the preamplifier was sent to a Cremat CR-200 shaping amplifier with a time constant of 100 ns. Although pulses from each detector were negative, the compensating circuit inverted one signal and produced large overshoots in both. Pulses from the detector facing the sample were positive-lobe-leading (PLL) bi-polar signals. The other detector produced negative-lobe-leading (NLL) pulses due to background γ-rays interacting with the detector or (n,α) events with the small amount of boron used as a dopant in the PIPS detector. An Agilent 12 bit digitizer (U1066A-001) was used to save waveforms and time stamps for each event, with a waveform consisting of 336 samples per event at 2.38 ns per sample, with 84 pre-trigger samples. The digitizer's full range ran from −1 V to 1 V, corresponding to raw digital values (RDV) of −2048 to 2047, respectively.

3. Data analysis

Data reduction was performed in two steps. First pulse shape analysis was performed to eliminate γ pile-up and "γ-flash" events. The pulse shape analysis method used in this work imposes two conditions based on the minimum and maximum samples. Minimum and maximum values were first found between samples 0 and 250 (~195 ns before the trigger threshold was exceeded to 400 ns after). To pass the first discrimination criteria the maximum and minimum samples were required to be

Table 2
Summary of samples parameters.

Sample	Oxide mass [mg]	Sample area [cm^2]	Average sample thickness [mg/cm^2]
Sm-147	9.6 ± 0.05	1.45 ± 0.08	6.6 ± 0.4
Sm-149	9.4 ± 0.05	1.55 ± 0.04	6.1 ± 0.2

Table 1
Isotopic fractions (percent) of samples as given by Oak Ridge Nation Laboratory [16]. Uncertainties not listed explicitly in this table are ± 0.01%.

Sample	Sm-144	Sm-147	Sm-148	Sm-149	Sm-150	Sm-152	Sm-154
Sm-147	0.05 ± 0.00	98.30 ± 0.05	0.85 ± 0.02	0.36	0.11	0.21	0.12
Sm-149	0.035	0.371	0.781	97.669 ± 0.03	0.571	0.392	0.181

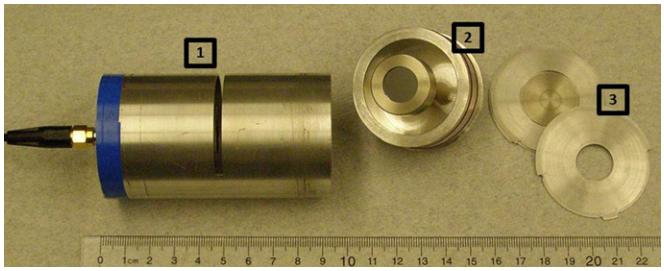

Fig. 1. Photograph of the detector chamber: (1) chamber shell, (2) one of the PIPS detectors, (3) sample holder. Aluminum tape was used to ground the shell. The sample holder is placed through the slit on the chamber shell.

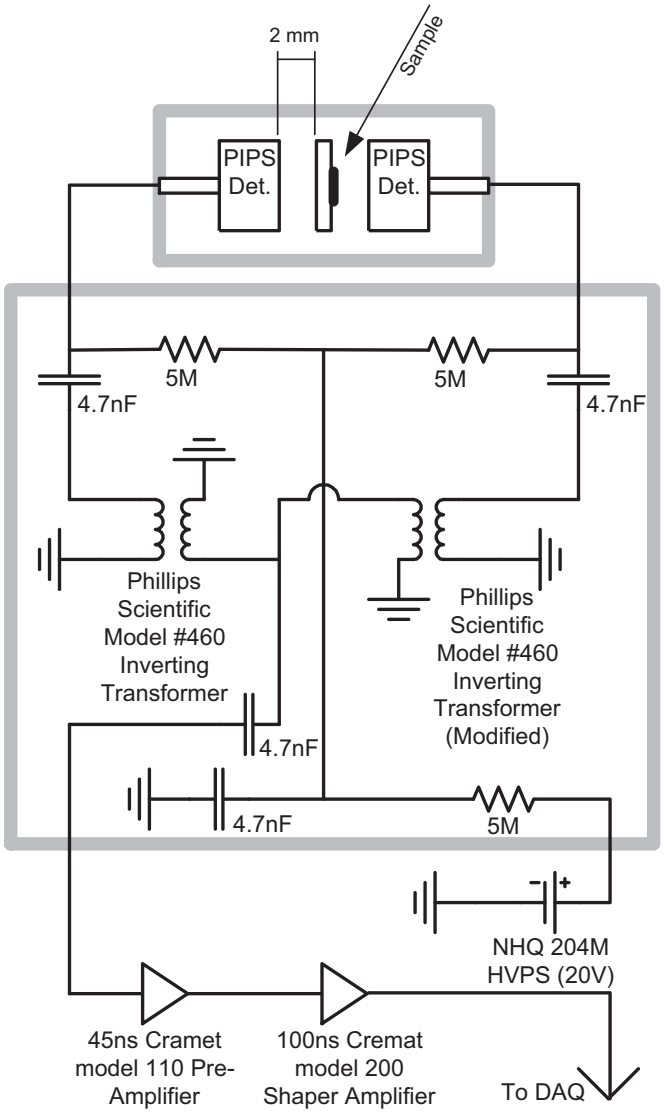

Fig. 2. Wiring diagram of the detector and electronics. The top box is the detector chamber shown in Fig. 1, the bottom box is the compensation circuit.

between 80 and 120 samples apart (~190 ns to ~286 ns apart). For PLL pulses the maximum occurred before the minimum and for NLL pulses the minimum occurred before the maximum. These limits were chosen from results obtained from an ^{241}Am source, shown in Fig. 3.

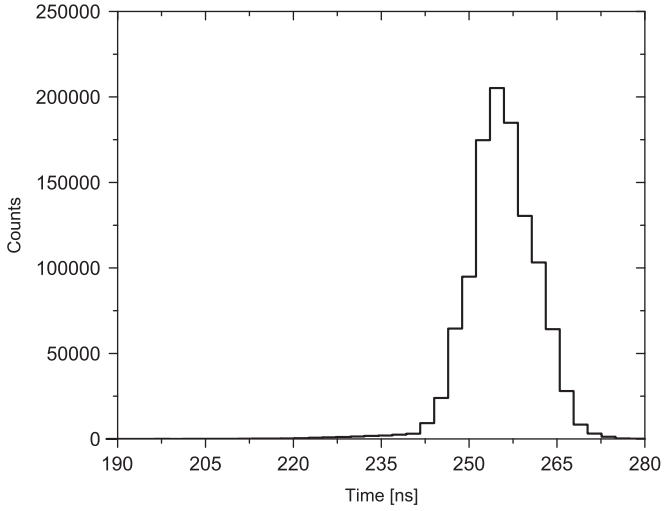

Fig. 3. Histogram of the time between the minimum and maximum samples recorded from an ^{241}Am source.

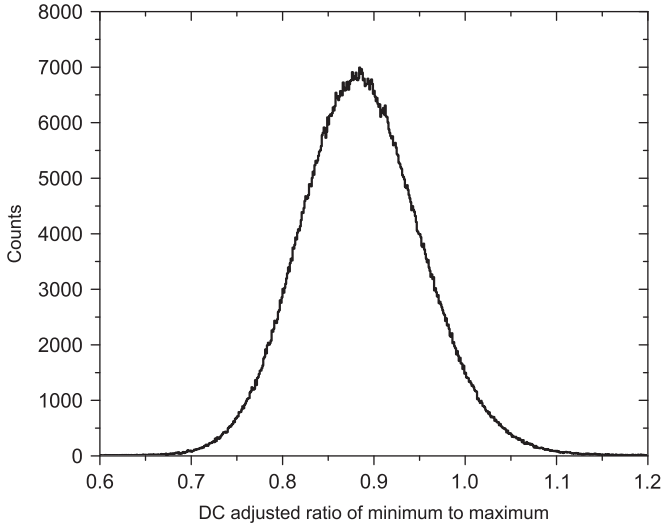

Fig. 4. Histogram of the ratio of maximum to minimum sample values adjusted for any DC offset from an ^{241}Am α source. Most α's from the ^{241}Am source meet the criteria given by Eq. (4).

The second condition is placed on the DC adjusted ratio of maximum to minimum values, or

$$0.6 \leq \left|\frac{MAX-Z}{MIN-Z}\right| \leq 1.2 \quad (4)$$

where *MAX* and *MIN* are the maximum and minimum sample values as a raw digital value (RDV), respectively. *Z* accounts for the DC offset and is computed as the average of the first 20 samples for PLL pulses. For NLL pulses, *Z* is the average of samples 180 to 199 corresponding to the 20 samples after the positive lobe of the pulse, roughly 229 ns to 274 ns after the trigger. Again, the ^{241}Am data was used to select these limits, see Fig. 4. Fig. 5 shows representative PLL pulses compared to noise pulses from the "γ-flash" and γ pile-up. Pulses failing either criterion were removed from further analysis.

PIPS detectors are constructed with a boron dopant that produces a low energy α background which are capable of passing the pulse shape criteria and required a second method of discrimination. *Q*-values of the (n,α) reactions in ^{147}Sm, ^{149}Sm and ^{10}B are 10.127, 9.436 and 2.789 MeV, respectively, so boron α events were easily removed through pulse height discrimination.

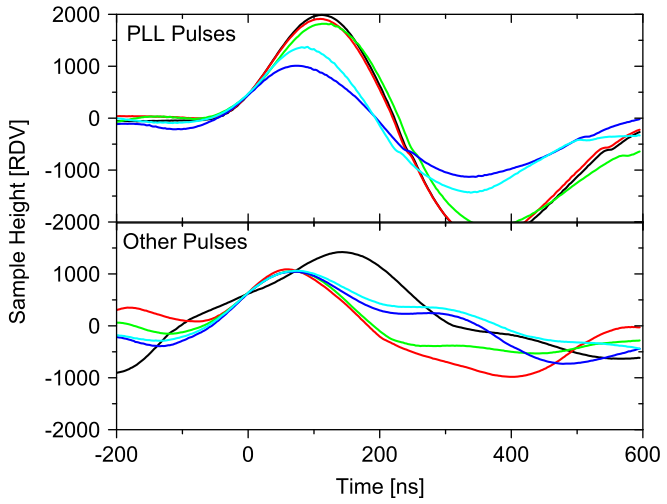

Fig. 5. Representative pulses for PLL caused by (n,α) reactions in samarium (top) and noise caused by the "γ-flash" and γ pile-up (bottom). The x-axis is time relative to the event trigger.

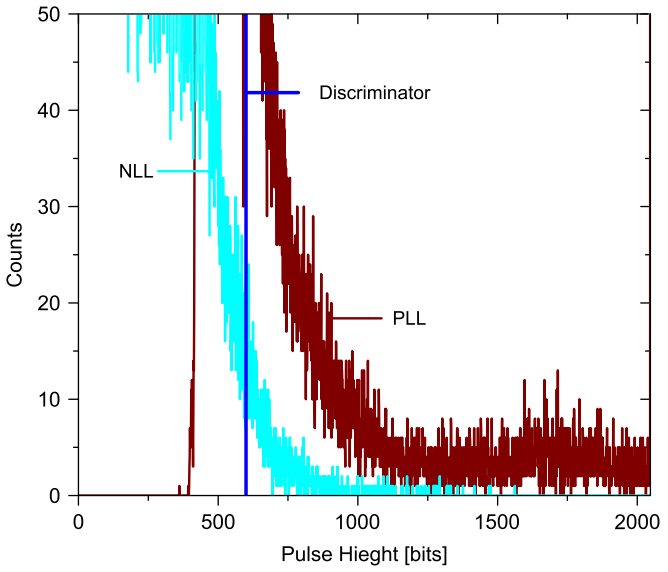

Fig. 6. Pulse height spectra of NNL (noise and boron only) and PLL (noise, samarium and boron) pulses for the ^{147}Sm run for all time of flights. Some PLL pulses were able to over-range the digitizer producing the peak at a RDV of 2047. Below a RDV of 600 the PLL and NLL lines overlap significantly.

Fig. 6 shows pulse height spectra from both detectors (PLL and NLL) during the ^{147}Sm run. All of the NLL events were caused by boron α's and the "γ-flash" so the lower limit discriminator value of 600 was chosen to eliminate the majority of NLL events. The remaining NLL's comprised the time-dependent background.

A time-independent background was taken as the count rate of PLL's from 2 to 4 ms. NLL counts were binned identically to the PLL counts and composed the time-dependent background. The total background rate was subtracted from the count rate.

The ^{147}Sm$(n,2\alpha)$ reaction releases an additional 1.91 MeV compared to the ^{147}Sm(n,α) reaction, and all other $(n,x\alpha)$ reactions for $x \leq 6$ are energetically possible with zero incident neutron energy. For ^{149}Sm, the Q-values for the $(n,2\alpha)$ and $(n,3\alpha)$ are 10.62 MeV and 11.91 MeV, respectively, and all other $(n,x\alpha)$ reactions for $x \leq 6$ are positive but smaller than 10 MeV. When the energy released during the reaction is divided between multiple α particles, each individual α possesses significantly less energy on average than during the (n,α) reaction. The likelihood that any single α particle can deposit enough energy in the detector to exceed the lower limit threshold is greatly reduced. Multiple α particles from a single $(n,x\alpha)$ reaction are less like to reach the detector than a single α particle, and energy lost in the sample would increase because the energy loss per α particle changes slowly as a function of energy in the few MeV range. The detector was incapable to discriminating events from different $(n,x\alpha)$ events, however the contribution from reactions with $x > 1$ is small due to lower α energies and no correction was made.

Energy deposition from charged particles lighter than α particles is limited by the detector's thin active volume. The lower limit discriminator was able to eliminate these events based on the pulse height criteria. Contribution from charged-particle-out reactions other than (n,α) were assumed to be negligible.

Time spectra from the ^{147}Sm measurement are shown in Fig. 7. Noise picked-up after the signals were combined caused ringing and limited the measurement without pulse shape discrimination to below 10 keV. As can be seen in Fig. 7, the combination of pulse shape and height discrimination eliminated much of the "γ-flash" counts in the high energy range and extended the measurement from $\sim$10 μs ($\sim$1 keV) to $\sim$1 μs ($\sim$100 keV).

The number of counts, C_i, from each sample over energy bin i can be calculated as

$$C_i = fN\sigma_i\Phi_i \tag{4}$$

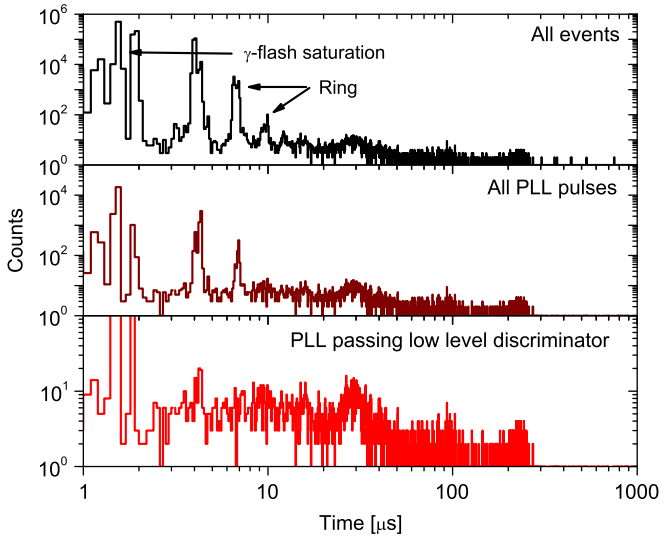

Fig. 7. Time spectra of counts from the ^{147}Sm measurement. The top plot is the spectra created by all triggers with no filtering, the middle plot is filtered to include only pulses passing the pulse shape analysis and the bottom plot is filtered by both pulse shape and pulse height.

where N is the number of samarium atoms in the sample as calculated from the sample mass, Φ_i (with units of cm^{-2}) is the integral of Eq. (2) over energy bin i, f is a normalization constant which includes the detector efficiency and flux normalization, and σ_i is the resolution-broadened cross section averaged over bin i. C_i is calculated from the measured events as

$$C_i = N_i^{PLL} - N_i^{NLL} - \Delta t_i(N_{BKG}^{PLL} - N_{BKG}^{NLL}) \tag{5}$$

where N_i^{PLL} and N_i^{NLL} are the recorded number of PLL and NLL pulses, respectively, over energy bin i, Δt_i is the width of bin i in seconds, N_{BKG}^{PLL} and N_{BKG}^{NLL} are the time-independent background counting rates of PLL and NLL pulses as measured between neutron pulses, respectively. The resolution-broadened cross

section over bin i was calculated as

$$\sigma_i = \frac{C_i}{fN\Phi_i} \tag{6}$$

The error in the σ_i was calculated from the uncertainties in N_i^{PLL}, N_i^{NLL}, N_{BKG}^{PLL}, N_{BKG}^{NLL} and the sample mass. The ^{147}Sm cross section measured here was normalized over the energy range 300 eV–2500 eV to the results obtained by Gledenov et al. [7] that were first broadened with the LSDS resolution using the method discussed by Danon [13]. The results from ^{149}Sm were normalized to the ^{147}Sm by the number of linac pulses and mass of the major isotope. Efficiency differences are small due to the small differences in atomic mass, sample thickness and Q-value for the two reactions.

4. Results

Fig. 8 shows the ^{147}Sm$(n,\alpha)^{144}$Nd cross section measured here compared to ENDF/B-VI.8, ENDF/B-VII, JENDL-3.3, JENDL-4.0 evaluations and the measurement by Gledenov et al. [7], all of which were broadened using the method described by Danon [13]. The new measurement presented here shows the best agreement with the shape of the measurement made by Gledenov et al. [7].

Fig. 9 shows the results of the ^{149}Sm$(n,\alpha)^{146}$Nd cross section compared to the broadened evaluations from ENDF/B-VII, JENDL-3.3 and JENDL-4.0. The measurement here lacks the structure predicted in both ENDF and JENDL below 10 eV. Some structure is present in the 10 eV–1 keV region but not to the degree that appears in the evaluations. It seems that due to lack of information the evaluated (n,α) cross section is a simple scaled down version of the total cross section. The lack of structure near the 0.0976 and 0.88 eV resonances would suggest that these resonances do not contribute significantly to the (n,α) reaction $(\Gamma_\alpha \ll \Gamma)$.

Large error bars are present in both measurements above 1 keV and in the ^{147}Sm measurement below $\sim$2 eV. The primary cause of the large error bars is from the counting statistics. Although the large error bars make it difficult to determine resonance parameters, the results are useful to compare gross structures and difference between different evaluations.

Despite the heavy filtering above 10 keV, the ^{147}Sm data show good agreement with ENDF/B-VII, JENDL-4.0 and Gledenov [7]

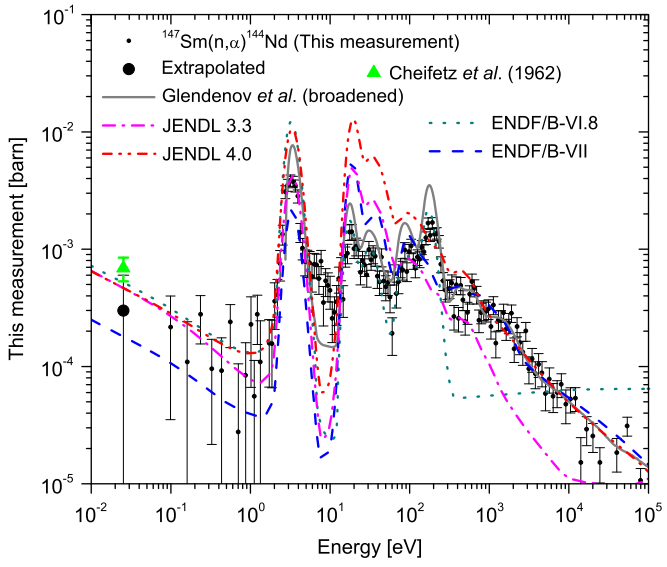

Fig. 8. Measured ^{147}Sm(n,α) cross section compared to previous measurements [7,17] and evaluations [18] broadened by the method given by Danon [13].

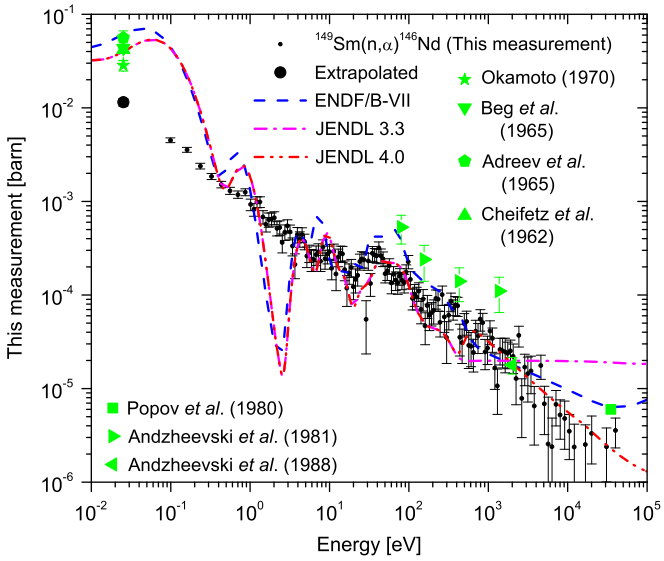

Fig. 9. Measured ^{149}Sm(n,α) cross section compared to previous measurements [17,19–24] and evaluations [18] broadened by the method given by Danon [13].

and the trends in ^{149}Sm agree with ENDF/B-VII from about 20 eV to 1 keV. The overall data trend is in good agreement with the previous measurement made by Popov [19] of <6 μbarn at 30 keV and the few measurements made by Andzheevski [22,23].

Data from 0.09 eV–1 eV were fitted to the equation $\sigma = AE^m$ using the nonlinear, iterative Levenberg–Marquardt method described by Press et al. [25] and taking the error in the measurement as the weight, where A and m are constants, and cross sections were extrapolated to values at 0.0253 eV. This model was chosen over the characteristic $1/v$ shape $(m=-0.5)$ because the low-lying or bound level resonances can cause deviations from the $1/v$ shape. The results of this extrapolation predict thermal cross section of 0.3 ± 0.3 mbarn for ^{147}Sm. The thermal cross section predicted here for ^{147}Sm is lower than the 0.69 ± 0.15 mbarn reported by Cheifetz [17]. Low count statistics below 1 eV from ^{147}Sm lead to the large uncertainty in the predicted thermal cross section and no correction was made for nearby resonance at 3.397 eV [18]. Using the same method, the results predict an 11.5 ± 1.1 mbarn thermal neutron cross section for ^{149}Sm. Okamoto [20] reported a 28.5 ± 3.7 thermal cross section, Cheifetz et al. [17], Beg and Macfarlane [21], and Andreev and Sirotkin [24] reported higher values closer to 43 mbarn. Again, this measurement predicted a slightly lower thermal cross section than previously measured. This extrapolation method was chosen because it best represents the effects of bound level (negative energy) resonances to the cross section.

The ^{147}Sm cross section is very low compared to the ^{149}Sm below 1 eV making a ^{149}Sm contamination of the ^{147}Sm sample a concern in this energy range. To eliminate any cross contamination from the two samples different glassware and pipettes were used and each contained only the one solution being disposed. The small amount of ^{149}Sm in the enriched ^{147}Sm sample (0.36%) contributes less than 5% of measured ^{147}Sm$(n,\alpha)^{144}$Nd cross section.

5. Conclusions

The high flux provided by the LSDS makes it is an obvious choice for measuring reactions with small cross sections on samples whose masses are required to also be small either due to the reaction of interest, expense of enrichment of natural material or limitations on the creation of radioactive isotopes.

Results from ^{147}Sm are in better agreement with Gledenov et al. [7] than with ENDF/B-VII. Extrapolation of the data presented for ^{149}Sm yields a thermal cross section of 11.5 ± 1.1 mbarn, which is smaller than the few thermal cross section points previously measured. This method demonstrates that (n,α) cross sections near 1 mbarn can be measured in a very reasonable amount of time (< 10 h per sample) with sample of only a few mg.

References

[1] P. Mohr, Physical Review C 61 (2000) 045802.
[2] S.E. Woosley, W.M. Howard, Astrophysical Journal Supplement Series 36 (1978) 285.
[3] M.H. Hadizadeh, S.M. Grimes, Nuclear Science Engineering 160 (2008) 207.
[4] T. Rauscher, Global transmission coefficients in Hauser-Feshback calculations for astrophysics,, in: M. Buballa, W. Nörenberg, J. Wambach, A. Wirzba (Eds.), Proceedings XXVIth International Workshop on Gross Properties of Nuclear Excitations, GSI, Darmstadt, 1998, p. 288.
[5] T. Rauscher, Prediction of nuclear reaction rates for astrophysics,, in: W. Hillebrandt, E. Müller (Eds.), Proceedings of the IX Ringberg Workshop On Nuclear Astrophysics, MPA, Garching, 1998, p. 84. MPA/P10.
[6] T. Rauscher, F.K. Thielemann, Global statistical model calculations and the role of isospin, in: A. Mezzacappa (Ed.), Stellar Evolution, Stellar Explosions, and Galactic Chemical Evolution, Institute of Physics, Bristol, 1998, p. 519.
[7] Yu.M. Gledenov, P.E. Koehler, J. Andrzejewski, K.H. Guber, T. Rauscher, Physical Review C 62 (2000) 042801(R) 62 (2000).
[8] P. Mohr, T. Rauscher, H. Oberhummer, Z. Mate, Z. Fulop, E. Somorjai, M. Jaeger, G. Staudt, Physical Review C 55 (1997) 1523.
[9] C. Wagemans, S. Druyts, P. Geltenbort, Physical Review C 50 (1994) 0556.
[10] A.A. Bergman, A.I. Isacoff, I.D. Murin, F.L. Shapiro, I.V. Shtranikh, M.V. Cazarnovky, "A Neutron Spectrometer Based on Measuring the Slowing-Down Time of Neutrons in Lead," Proceedings of the International Conference on the Peaceful Uses of Atomic Energy, pp. 135, August 1955.
[11] E. Anders, N. Grevesse, Geochimica et Cosochimica Acta 53 (1989) 197.
[12] G. Zhang, J. Zhang, L. Guo, H. Wu, J. Chen, G. Tang, Yu.M. Gledenov, M.V. Sedysheva, G. Khuukhenkhuu, P.J. Szalanski, Applied Radiation and Isotopes 67 (2009) 46.
[13] Y. Danon, R.E. Slovacek, R.C. Block, R.W. Lougheed, R.W. Hoff, M.S. Moore, Nuclear Science and Engineering 109 (1991) 341.
[14] H.M. Fisher, "Monet Carlo Feasibility Assessment of the Lead Slowing Down Time Spectrometer for Spent Fuel Assay and Fuels Management", Ph.D. Thesis, Rensselaer Polytechnic Institute.
[15] R.E. Slovacek, D.S. Cramer, E.B. Bean, J.R. Valentine, R.W. Hockenbury, R.C. Block, Science and Engineering 62 (1977) 455.
[16] B. Benton, Personal communication.
[17] E. Cheifetz, J. Gilat, A.L. Yavin, S.G. Cohen, Physics Letters 1 (7) (1962) 289.
[18] National Nuclear Data Center Website, Evaluated Nuclear Data Files, ⟨http://www.nndc.bnl.gov/exfor/endf00.jsp⟩, retrieved September, 2010.
[19] Yu. Popov, V. Salatskij, G. Khuukhenkhuu, Soviet Journal of Nuclear Physics 32 (4) (1980) 459.
[20] K. Okamoto, Nuclear Physics A 141 (1) (1970) 193.
[21] K. Beg, R.D. Macfarlane, Bulletin of the American Physical Society 10 (6) (1965) 724.
[22] Yu. Andzheevski, V.P. Vertenbnyĭ, Vo Kim Tkhan, V.A. Vtyurin, A.L. Kirilyuk, Yu.P. Popov, Yad. Fiz. 48 (20) (1988).
[23] J. Andzheevski, Vo Kim Tkhan, V.A. Vtyurin, A. Koreiwo, Yu.P. Popov, M. Stempinsky, Yad. Fiz. 32 (1980) 1496.
[24] V.N. Andreev, S.M. Sirotkin, Soviet Journal of Nuclear Physics 1 (2) (1965) 177–185.
[25] W.H. Press, S.A. Teukolsky, W.T. Vetterling., B.P. Flannery, Numerical Recipes: The Art of Scientific Computing, third ed., Cambridge University Press, 2007.